Volume 12
Number 4
28 January 2020
Pages 2161-2834

Nanoscale

rsc.li/nanoscale

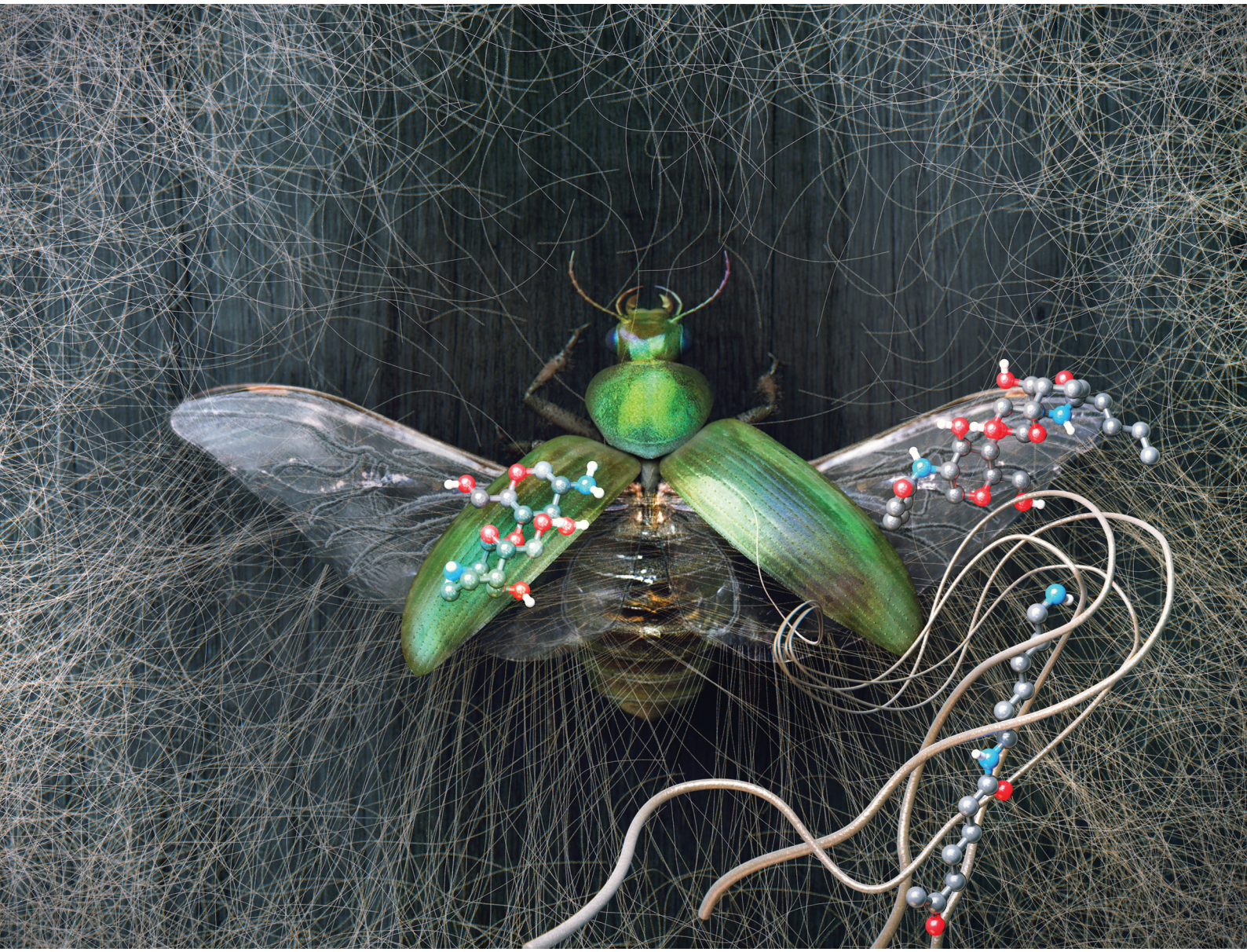

ISSN 2040-3372

ROYAL SOCIETY OF CHEMISTRY

PAPER
Sung Yeon Hwang, Dongyeop X. Oh, Jeyoung Park *et al.*
Rediscovery of nylon upgraded by interactive biorenewable nano-fillers

NCNST

Published on 11 November 2019. Downloaded by Korea Research Institute of Chemical Technology (KRICT) on 1/10/2023 6:07:26 AM.

Nanoscale

PAPER

View Article Online
View Journal | View Issue

Check for updates

Cite this: *Nanoscale*, 2020, **12**, 2393

Rediscovery of nylon upgraded by interactive biorenewable nano-fillers†

Lam Tan Hao, ‡[a,b] Youngho Eom, ‡[a,c] Thang Hong Tran, [a,b] Jun Mo Koo, [a] Jonggeon Jegal, [a] Sung Yeon Hwang, *[a,b] Dongyeop X. Oh *[a,b] and Jeyoung Park *[a,b]

Inorganic nanomaterials can only stiffen nylon with a significant loss of its toughness and ductility. Furthermore, they are not eco-friendly. In this study, the facile tuning of nylon's mechanical properties from stiff to tough was achieved, using cellulose nanocrystals (CNC) and chitosan nanowhiskers (CSW) as biorenewable fillers. The interaction between the matrix and filler was controlled by varying the types of fillers and the employed processing methods, including *in situ* interfacial polymerization and post-solution blending. Particularly with CSW, the *in situ*-incorporated filler with a 0.4 wt% loading strengthened nylon and led to a 1.9-fold increase in its Young's modulus (2.6 GPa) and a 1.7-fold increase in its ultimate tensile strength (106 MPa), whereas the solution-blended filler with a 0.3 wt% loading toughened the polymer with a 2.1-fold increase (104 MJ m^{-3}). Compared with inorganic nanocomposites, these interactive biofiller-nanocomposites are unrivaled in their reinforcing performance when normalized by filler content. This stiff-to-tough tuning trend is more pronounced in the CSW system than in the CNC system. Covalent polymer grafts on the amine surface of CSW enhanced interfacial interactions in the *in situ* method, whereas its cationic surface charges plasticized the polymer matrix in the blending method. This proteinaceous composite-mimicking all-organic nylon nanocomposite opens new possibilities in the field of reinforced engineering plastics.

Received 19th September 2019,
Accepted 10th November 2019

DOI: 10.1039/c9nr08091k

rsc.li/nanoscale

Introduction

Plastics have become an indispensable part of our daily life owing to their favorable properties such as light weight, low cost, high flexibility, and easy processing.[1–3] However, the mechanical properties of neat plastics do not always meet the technical requirements for applications under extreme conditions. The demand for light, but structurally strong and stiff materials is one such requirement, which has driven the development of organic–inorganic hybrid materials, widely known as inorganic filler-reinforced nanocomposites.[4–6] These materials generally consist of a polymer matrix, and at least one inorganic component in a sub-micrometric, usually nanometric, size for enhanced efficiencies, *e.g.*, clays,[7] and carbon nanomaterials.[8,9]

Despite their immense value, the use of hybrid nanocomposites is not encouraged in the current sustainable industrial era as they create serious environmental and health problems. Most nanocomposite wastes are disposed through landfills or incineration,[10,11] and, upon burning, they produce fine particulates, which cannot be further pyrolyzed.[12] Long-term occupational exposure and inhalation of such inorganic particulates has been strongly linked to multiple pulmonary effects, inflammation, and carcinogenesis.[13,14]

Furthermore, the hybrid materials face technological limitations. They are only able to exhibit high mechanical properties and express novel functionalities when the interfacial area between the constituents is maximized and the dispersion state of the filler within the matrix is controlled. In terms of mechanical performance, the homogeneous dispersion of nanofillers is prerequisite to the reinforcing effect because the larger fraction of the adsorbed polymer chains on the surface of the filler results in the higher reinforcing effectiveness.[4,15] In terms of other functional performances such as electrical, thermal and optical properties, however, a specific dispersion state of nanomaterials should be required to develop a percolated network or anisotropically arranged structure *via* self-

[a]*Research Center for Bio-based Chemistry, Korea Research Institute of Chemical Technology (KRICT), Ulsan 44429, Republic of Korea. E-mail: crew75@krict.re.kr, dongyeop@krict.re.kr, jypark@krict.re.kr*
[b]*Advanced Materials and Chemical Engineering, University of Science and Technology (UST), Daejeon 34113, Republic of Korea*
[c]*Department of Polymer Engineering, Pukyong National University, Busan, 48513, Republic of Korea*

†Electronic supplementary information (ESI) available: Characterization details of Ny66 composite films; Fig. S1–S7; Tables S1–S5. See DOI: 10.1039/c9nr08091k

‡These authors contributed equally.

Published on 11 November 2019. Downloaded by Korea Research Institute of Chemical Technology (KRICT) on 1/10/2023 6:07:26 AM.

assembly. To achieve this goal, the inorganic nanoparticles should undergo the surface modification process including the polymeric grafting or acid treatment before the *ex situ* mixing.[16–18] However, in most cases, the unmodified inorganic particles are poorly or randomly dispersed in the organic polymeric matrices because of the weak interaction between organic and inorganic materials, thus making the preparation of true nanocomposites a significant challenge.[9] Moreover, whereas inorganic nanomaterials stiffen the matrix, they inherently bring about a large reduction in toughness and ductility of the polymeric material.

At the same time, researchers may learn from all-organic nanocomposites in nature that continue to inspire the scientific community. For example, mineral-deficient load-bearing tissues of invertebrate organisms have attracted considerable attention as high-performance and mechanically tunable biomaterials. The proteinaceous matrix in these tissues is reinforced with natural nanofiber-structural fillers such as cellulose or chitin, which have an elastic modulus of 120–150 GPa.[19,20] Tunicates, which belong to a marine invertebrate family, have a hard, yet tough, protective shell, which is composed of interactively bonded cellulose nanofibers and proteins, forming a reinforced organic complex.[21–23] Similarly, certain parts of insect exoskeletons and cephalopod beaks are extremely hard and stiff, whereas other parts are soft and tough; these remarkable variations are enabled by the controlled degree of coupling density between chitin-binding proteins and strong chitin nanofibers.[20,24] From a material engineering perspective, these nano-scaled cellulose and chitin, which are naturally abundant, biodegradable, and biocompatible, are highly appealing as renewable and sustainable material sources.[25–28]

Even though these two bio-renewable nanofillers have been incorporated for enhancing the mechanical properties of several polymers, the resulting materials often have inadequate characteristics because of poor dispersion of the filler.[25–27,29–32] Furthermore, fabrication of polyamide (nylon) nanocomposites with bio-renewable nanofillers is particularly challenging. The mechanical reinforcing effects achieved are insignificant considering the amount of filler added, as the thermal requirement for nylon composite melt-processing is close to the degradation temperature of the nanocellulose materials.[33–35] Additionally, the homogeneous dispersion of these nanofillers within the strongly hydrogen-bonded polymer matrices is highly challenging. Even though chitosan nanowhiskers (nanochitin-derived materials) are expected to exhibit effective hydrogen bonding with nylon, no successful results of such use have been reported yet.

Herein, we report the preparation of strong and mechanically tunable novel all-organic nanocomposites through *in situ* polymerization and post-solution blending approaches. This is achieved by emulating bio-hardening mechanisms and stiff-to-tough transition of natural nanofiber-reinforced proteinaceous composites. We chose nylon 6, 6 (Ny66), an aliphatic polyamide, as the matrix material for the study, because of its inherent ability to mimic natural proteinaceous materials such as silk. For the first time, comparative filler-effects of cellulose nanocrystals (CNC) and chitosan nanowhiskers (CSW), which were extracted from renewable biomasses, on the Ny66 nanocomposite properties were investigated under the same preparation conditions. Using an *in situ* interfacial polymerization process of hexamethylenediamine-alkaline aqueous solution pre-dispersed with nanofillers and adipoyl chloride-organic solution, strong interactions are expected to occur between the polymers and organic nanomaterials (Fig. 1a). Additionally, Ny66 was mixed with CNC or CSW by solution blending in formic acid (Fig. 1b). The type of filler and composite preparation method influenced the degree of intermolecular hydrogen bonding and the arrangement of the polymer chains and allowed the tunable mechanical reinforcement of the composites. Furthermore, these interactive all-organic nanocomposites are excellent alternatives to circumvent the limitations imposed by the passive inorganic–organic hybrid materials.

Results and discussion

Preparation of Ny66 nanocomposite films with biorenewable nanofillers

The surface characteristics of biorenewable nanofillers are easily tailorable even with simple environmental controls, due to the presence of abundant surface polar functional groups and their facile chemical accessibility. Such organic additives with adjustable surface features are expected to provide remarkable interfacial affinity and reinforcing behavior to a polymer matrix that cannot be realized with conventional inorganic filler-based composites. CNC derived from sulfuric acid hydrolysis of wood pulp have an approximate diameter and length of 5–20 nm and 100–200 nm, respectively.[36,37] On the other hand, CSW obtained from demineralized shrimp shells by acidic hydrolysis followed by alkaline deacetylation were 150–250 nm long and 10–25 nm wide (Fig. S1 in the ESI†).

To evaluate the influence of different types of biorenewable nanofillers and preparation methods on nanocomposite properties, we prepared four different series of Ny66 nanocomposites at considerably low filler concentrations (0.1–0.5 wt%) (Fig. 1a and b). There have been attempts to introduce the biorenewable filler like CNC into polyamides *via in situ* polymerization.[38–40] However, preparation of the test specimen still required melt processing.[40] This could lead to an underestimation of the actual reinforcing effectiveness of the filler because the high melting point of most polyamides exceeds the degradation temperature of CNC. In this study, we successfully fabricated *in situ* polyamide composites containing bioreneweable fillers including CNC and CSW without thermal application, thus minimizing the degradation of the fillers.

The *in situ* polymerization is regarded as one of the most effective methods for producing high-performance nanocomposites because it enables the incorporation of the nano-

 This journal is © The Royal Society of Chemistry 2020

Published on 11 November 2019. Downloaded by Korea Research Institute of Chemical Technology (KRICT) on 1/10/2023 6:07:26 AM.

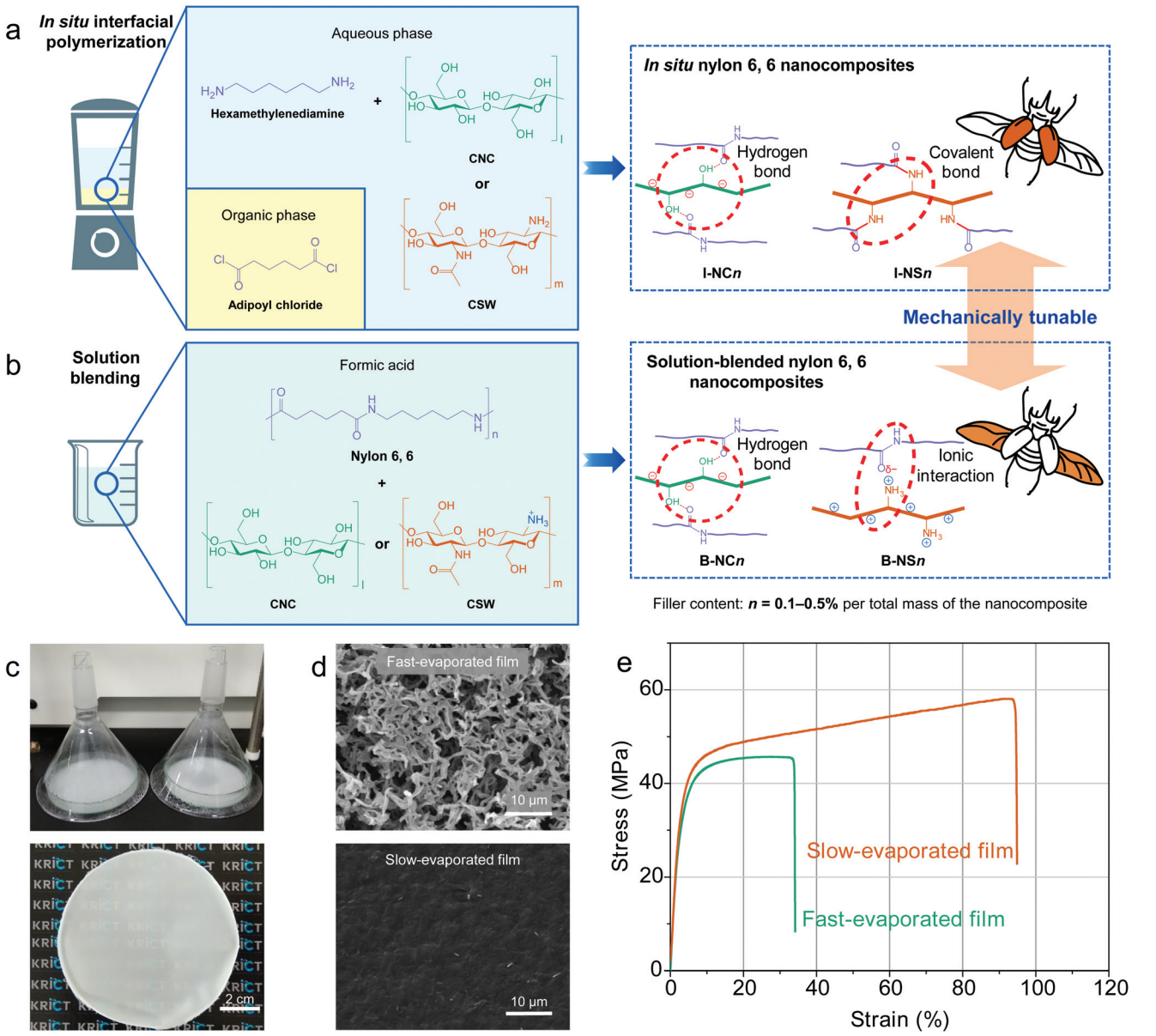

Fig. 1 Schematic illustration for the preparation of Ny66 nanocomposite films containing CNC or CSW *via* (a) *in situ* interfacial polymerization or (b) solution blending in formic acid. The mechanical properties of I-NS and B-NS series, representing the hard elytra and the soft back wings of a scarab beetle, respectively, can be tunable, as opposed to the I-NC and B-NC series. (c) Photographs of the solution casting procedure and as-prepared film. A glass funnel was used to control the evaporation rate of formic acid. (d) Scanning electron microscope (SEM) images showing the difference in surface morphology of films prepared from fast and slow evaporation of formic acid. (e) Representative tensile stress–strain curves of neat Ny66 films depending on the solvent evaporation rate.

filler into the polymer matrix while preserving its superior dispersion.[41,42] Whereas conventional carbon-based nanofillers such as single- or multi-walled carbon nanotubes are appealing, they require functionalization or the use of a surfactant to enhance their dispersibility in the monomer-containing reaction medium.[6,43–46] In this study, however, the inherently strong hydrophilicity of CNC and CSW allows their excellent dispersion in the aqueous phase without the need for any pretreatment, thus simplifying the composite preparation process.

To facilitate film processing, the concentration ratio of the two monomers in the polymerization system was adjusted for preparing Ny66 of sufficiently high molecular weight.[47] Indeed, the viscosity average molecular weight (M_v) of the prepared Ny66, which was isolated from the composites by syringe-filtration is similar to that of the neat Ny66 (28–34 kg mol^{-1}, Table S1 in the ESI†) and is comparable to commercial Ny66 pellets (38 kg mol^{-1}). These results suggest that incorporation of CNC and CSW had a negligible effect on the M_v of the composites. In another approach, the solution-blended nano-

Published on 11 November 2019. Downloaded by Korea Research Institute of Chemical Technology (KRICT) on 1/10/2023 6:07:26 AM.

composites were prepared by dissolving the neat Ny66 with freeze-dried CNC or CSW in formic acid, followed by vigorous mixing and solvent evaporation. Given the variable surface features of the natural fillers, CNC is negatively charged due to the sulfation of several C6 hydroxyl groups.[48,49] However, the C2 amine groups (1.15 mmol g^{-1}, degree of deacetylation of 70%)[26] of the CSW are positively charged by formic acid during solution blending. Furthermore, these amine groups are reactive towards the –COCl groups of adipoyl chloride in the amide coupling reaction, which facilitates the facile grafting of Ny66 chains onto the filler during polymerization. The resulting distinct surface features would lead to different interfacial interactions and reinforcement behaviors of the composite systems. The nanocomposite series prepared *in situ* by varying the wt% of the nanofillers is denoted I-NC*n* for CNC, and I-NS*n* for CSW, respectively, whereas the solution-blended nanocomposite series are coded as B-NC*n* for CNC, and B-NS*n* for CSW, respectively, where *n* is wt% of nanofiller with respect to total mass of the composite (Fig. 1).

Ny66 films were prepared by solution casting and subsequent evaporation using formic acid as the solvent (Fig. 1c), and the resulting films had an average thickness of 0.13–0.16 mm. Unfortunately, these films were found to be porous and brittle and exhibited poor mechanical properties due to the fast solvent evaporation (Fig. S2 in the ESI†), which is in line with the results reported previously.[50] However, to obtain a high-quality film, we reduced the formic acid evaporation rate by covering the solution-casted dish with a simple long-neck glass funnel. As a result, the "slow-evaporated" film showed a continuous surface without a porous structure, and afforded a 1.4-fold higher ultimate tensile strength (σ) of 61 MPa and a 2.7-fold higher elongation at break (ε_b) of 93% compared with those of the "fast-evaporated" film (44 MPa and 34%, respectively), as shown in Fig. 1d and e. The surface morphology at different positions of the fractured film was investigated, and the results are explained in the ESI.† Given the better properties of the film obtained under the controlled conditions, all the Ny66 nanocomposite films were processed by the slow-evaporation technique, so that their mechanical properties could be compared appropriately.

Tuning the mechanical properties of Ny66 nanocomposites

As the amine groups of CSW are readily protonated under acidic pH, the interfacial interactions in the CSW and CNC-containing Ny66 composites will be different when formic acid is used for film processing. The mechanical properties of the prepared four different types of Ny66 nanocomposites are presented in Fig. 2 and Table S2 in the ESI.† The values for tensile properties, including Young's modulus (E), σ, and ε_b of the prepared lab-scale neat Ny66 were within 88–94% of those of the commercial sample (Table S2 in the ESI†) and were in good agreement with previously reported values.[51,52]

In case of the Ny66/CNC nanocomposites, incorporation of the nanofiller *via* either preparation method led to an increase in E and σ at the cost of ε_b, thereby improving the stiffness of the composite systems, which is in line with the typical reinforcement behavior of polymer nanocomposites.[35,45,46,50] The matrix-filler interfacial interaction resulting from the hydrogen bonding between the –OH groups of the CNC and the amide groups of the surrounding Ny66 chains could be responsible for the strengthening of the composite systems.[53,54] Such reinforcement is more noticeable in the films prepared using the *in situ* method, compared with those prepared by solution-blending with the same filler loading, which indicates that the direct incorporation of the CNC filler from the polymerization media leads to its higher entanglement with Ny66 chains due to the better dispersion. This reinforcing effect was maximized at 0.4 wt% loading of the filler; I-NC0.4 exhibited a 1.6-fold increase in both E (2.2 GPa) and σ (100 MPa), whereas a 1.4-fold increase was observed for those properties in B-NC0.4, compared with those of the neat Ny66, respectively. Given the difference in reinforcement efficiency between two preparation methods, it is reasonable to suggest that the *in situ* polymerized Ny66 chains in the vicinity of CNC were successful in preventing the aggregation of the nanomaterials, which facilitated better dispersion of the CNC filler, thereby leading to the formation of stronger interfacial hydrogen bonds and a superior strengthening effect than those of the post-blended nanocomposites.

Compared with the monotonous increase in the stiffness of the CNC-containing composites, the mechanically tuned nylon films employing CSW as the nanofiller can display the beneficial stiff-to-tough transition depending on the preparation routes used during their synthesis. The *in situ* Ny66/CSW nanocomposites exhibited a similar trend with the CNC systems, but the reinforcement effect of the CSW was greater than that of the CNC at the same filler loading. Indeed, I-NS0.4 exhibited a 1.9-, and 1.7-fold increase in E (2.6 GPa), and σ (106 MPa), respectively. This stronger effect seems to result from the synergistic contribution of the covalently cross-linked polymer grafting and the physical hydrogen bonding interactions. As mentioned before, the $-NH_2$ groups on the CSW surface can produce polymeric branches upon reacting with the adipoyl chloride's –COCl groups during polymerization. In addition, the abundant –OH and residual NH_2 groups of CSW can form hydrogen bonds with the amide groups of Ny66, which could be comparable in strength as those of the CNC's –OH groups, and the resulting stronger physical confinement of the filler-entangled polymer chains afford the higher tensile modulus.

Interestingly, in contrast to the *in situ* composites, Ny66 was considerably toughened by the post-solution blending with CSW, and displayed a simultaneous increase in σ up to 80 MPa (1.3-fold at 0.4 wt%) and ε_b up to 147% (1.6-fold at 0.3 wt%). This remarkable result of the B-NS series can be ascribed to the formation of the $-NH_3^+$ groups on the CSW surface *via* formic acid protonation during the film processing, which was confirmed by the results from the Fourier-transform infrared spectroscopy (FTIR) and titrimetric analysis of these samples (Fig. S3 in the ESI†). Charged nanomaterials tend to act as plasticizers *via* electrostatic repulsions and promote the disentanglement of the polymer chains and subsequent stretching

 This journal is © The Royal Society of Chemistry 2020

Published on 11 November 2019. Downloaded by Korea Research Institute of Chemical Technology (KRICT) on 1/10/2023 6:07:26 AM.

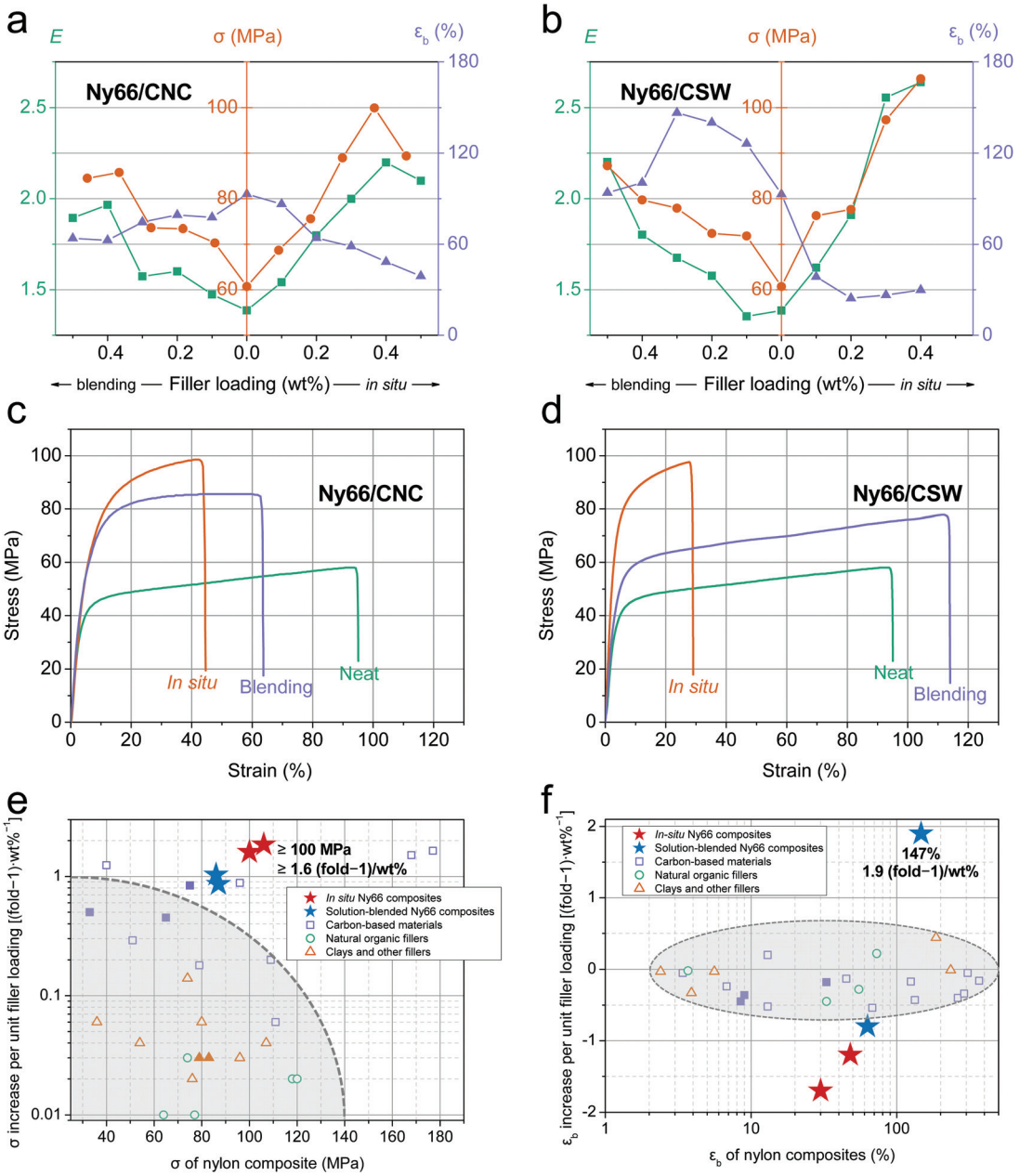

Fig. 2 Variation of mechanical properties including Young's modulus (E, ■), ultimate tensile strength (σ, ●), and elongation at break (ε_b, ▲) with the varied filler content of (a) Ny66/CNC and (b) Ny66/CSW nanocomposites. Representative stress–strain curves of (c) Ny66/CNC and (d) Ny66/CSW nanocomposites at a filler loading of 0.4 wt%. Ashby plots of (e) σ increase and (f) ε_b increase per unit (1 wt%) filler loading [(fold − 1) wt%$^{-1}$] of Ny66 nanocomposites in this study and other polyamide composites reported in the literature (Table S3†). The red and blue star symbols represent the *in situ* and solution-blended Ny66 composites in the current study, respectively.

under tension. This behavior delays the failure and, as a result, produces tougher nylon films with an elevated ε_b.[49,55] In this regard, the contrasting behavior of CSW in the I-NS series implies that the *in situ*-incorporated CSW filler was negligibly protonated during dissolution in formic acid because of the polymeric wrapping and grafting onto the surface resulting from the amidation of the free NH_2 groups.

To assess the reinforcing effectiveness of CNC and CSW on Ny66, we compared the increase in σ and ε_b per unit (1 wt%) filler loading [(fold − 1) wt%$^{-1}$] for these two nanofillers, with the literature data for polyamide composites obtained with other types of fillers.[56] Detailed data for polyamide composites reinforced by CNC, CSW, and other fillers are summarized in Table S3 in the ESI,† and plotted in Fig. 2e and f. The four types of films prepared in this study achieved a record σ of >85 MPa using the post-blending, and ≥100 MPa using the *in situ* polymerization. Furthermore, improved reinforcement performance [1.9 (fold − 1) wt%$^{-1}$] and the highest ε_b (147%)

Published on 11 November 2019. Downloaded by Korea Research Institute of Chemical Technology (KRICT) on 1/10/2023 6:07:26 AM.

were observed for the B-NS film, although this parameter was shown to decrease in most polyamide composites with an increase in E and σ. The mechanically reinforcing effectiveness of CNC and CSW is comparable to that of functionalized single-walled carbon nanotubes on nylon 610, which were prepared using *in situ* polymerization.[45] Overall, CNC and CSW are eco-friendly and offer distinct advantages in terms of convenient and cost-effective processing, without the need for surface modifications. Considering that the facile tunability of the mechanical properties of nylon has been achieved, these natural nanomaterials could serve as alternatives to the inorganic and carbon-based reinforcing fillers in composite processing.

Structural analysis of uniaxial deformation and interfacial interaction

The morphological changes of the tensile-fractured specimens can be studied from the SEM images (Fig. 3) of the representative composite samples with the 0.4 wt% filler loading at three different positions, including the grip, whitening, and fractured regions (Fig. 3a). The corresponding two-dimensional small-angle X-ray scattering (2D SAXS) patterns are also included in each image to inform the microstructural deformation during tensile testing.

At the grip position, all the composite films exhibited a smooth surface, and their 2D SAXS pattern around the beam stop was almost isotropic due to the lack of tensile deformation (Fig. 3b). Interestingly, I-NS0.4 showed bundles of muscle-like fibers, indicating robustness. As the measuring position got closer to the fractured cross-section, elongated microvoids, which bring about the whitening of the specimens, were observed along the tested direction (Fig. 3c). The ellipsoidal shape of the SAXS scattering with anisotropy perpendicular to the tested direction is direct evidence of the elongation and orientation of the internal microvoids.[57] Among the tested samples, a noticeable ellipsoidal pattern of

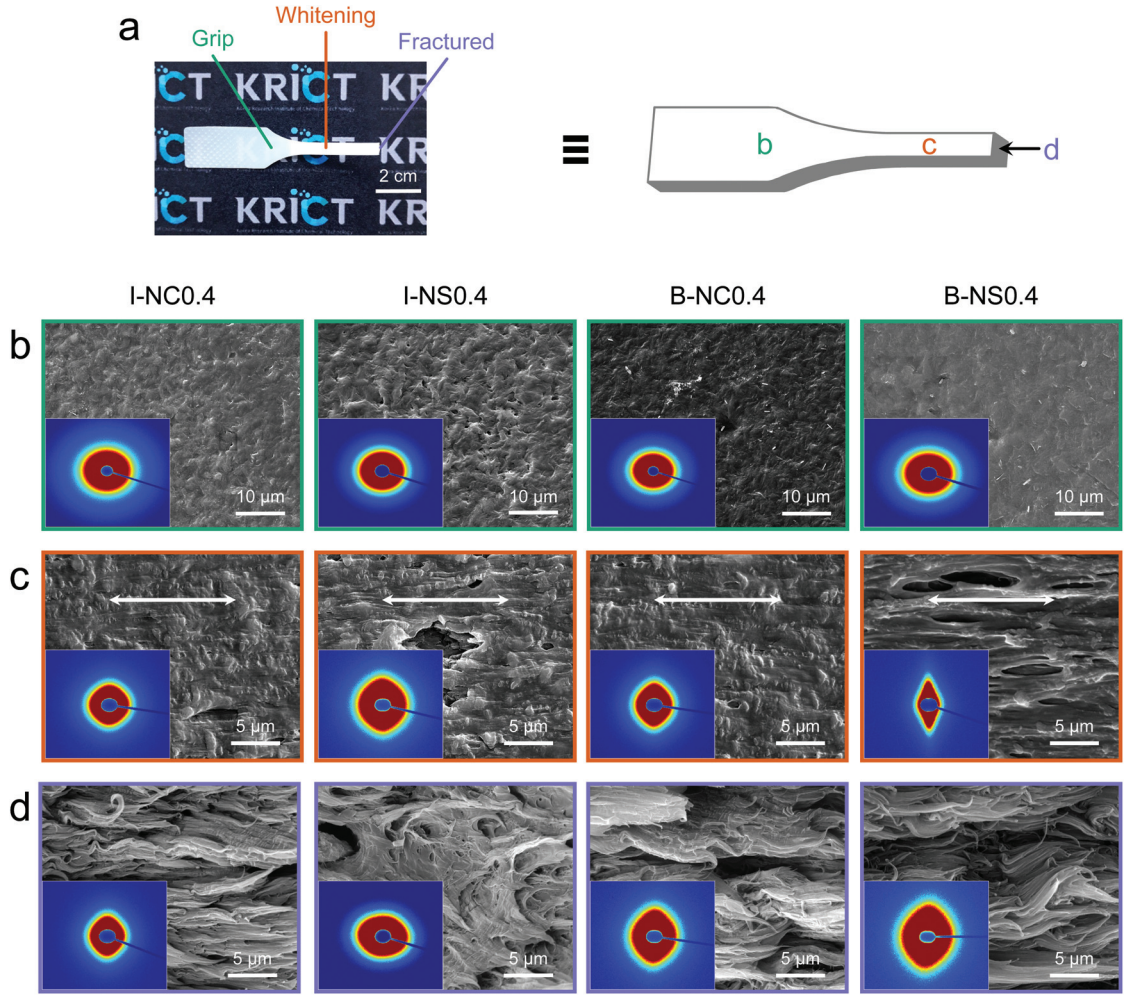

Fig. 3 (a) Photograph and illustration of a Ny66 film specimen after tensile testing, showing the three regions measured using SEM and SAXS. SEM images of (b) grip, (c) whitening (necking), and (d) fractured cross-section positions (from left to right) of I-NC0.4, I-NS0.4, B-NC0.4, and B-NS0.4 films at the nanofiller loading of 0.4 wt% upon tensile testing. The double-headed white arrows in (c) indicate the direction of the stretching force. Insets are their respective 2D SAXS images.

 This journal is © The Royal Society of Chemistry 2020

Published on 11 November 2019. Downloaded by Korea Research Institute of Chemical Technology (KRICT) on 1/10/2023 6:07:26 AM.

the scattering was observed for B-NS0.4, which is a result of a large extension caused by stable necking, as well as the delayed failure. This morphological change has a close relation to the higher ε_b value of the B-NS0.4 (strongly toughened sample) compared with other composite systems. On the other hand, the scattering anisotropy at the whitening position for the *in situ* composites is relatively low, which suggests that the well-dispersed nanofillers strongly disturb the rearrangement and orientation of the polymer chains under uniaxial tension. The fibrous structure at the fractured surface was developed during tensile testing, but their relaxation after failure resulted in the reduction of the anisotropy of the SAXS scattering pattern (Fig. 3d). Remarkably, the disordered fibers were fused in I-NS0.4 due to the binder-type properties of the graft-containing CSW, which were indicated by the presence of the most isotropic 2D SAXS pattern among other samples.

The wide-angle X-ray scattering (WAXS) results of the CSW-containing Ny66 composites are compared to clearly elucidate the effects of preparation methods and the corresponding interfacial interactions on the microstructural deformation. The deconvoluted one-dimensional (1D) and 2D WAXS patterns of the neat samples and the four types of the composites at the three measurement positions are shown in Fig. S4 and S5 in the ESI.† The 1D WAXS patterns of I-NS0.4 showed similar X-ray patterns at the three positions (Fig. 4b), whereas the neat Ny66 and B-NS0.4 samples exhibited a sharp decrease in the intensity at the deformed regions (whitening and fractured) compared with that of the grip spot (Fig. 4a and c). The broadening, as well as reduced intensity of the two prominent peaks at 20.2 and 24.4°, indicated the dissociation of hydrogen bonding of the nylon chains and the subsequent rearrangement of crystallites because the crystal structure for such

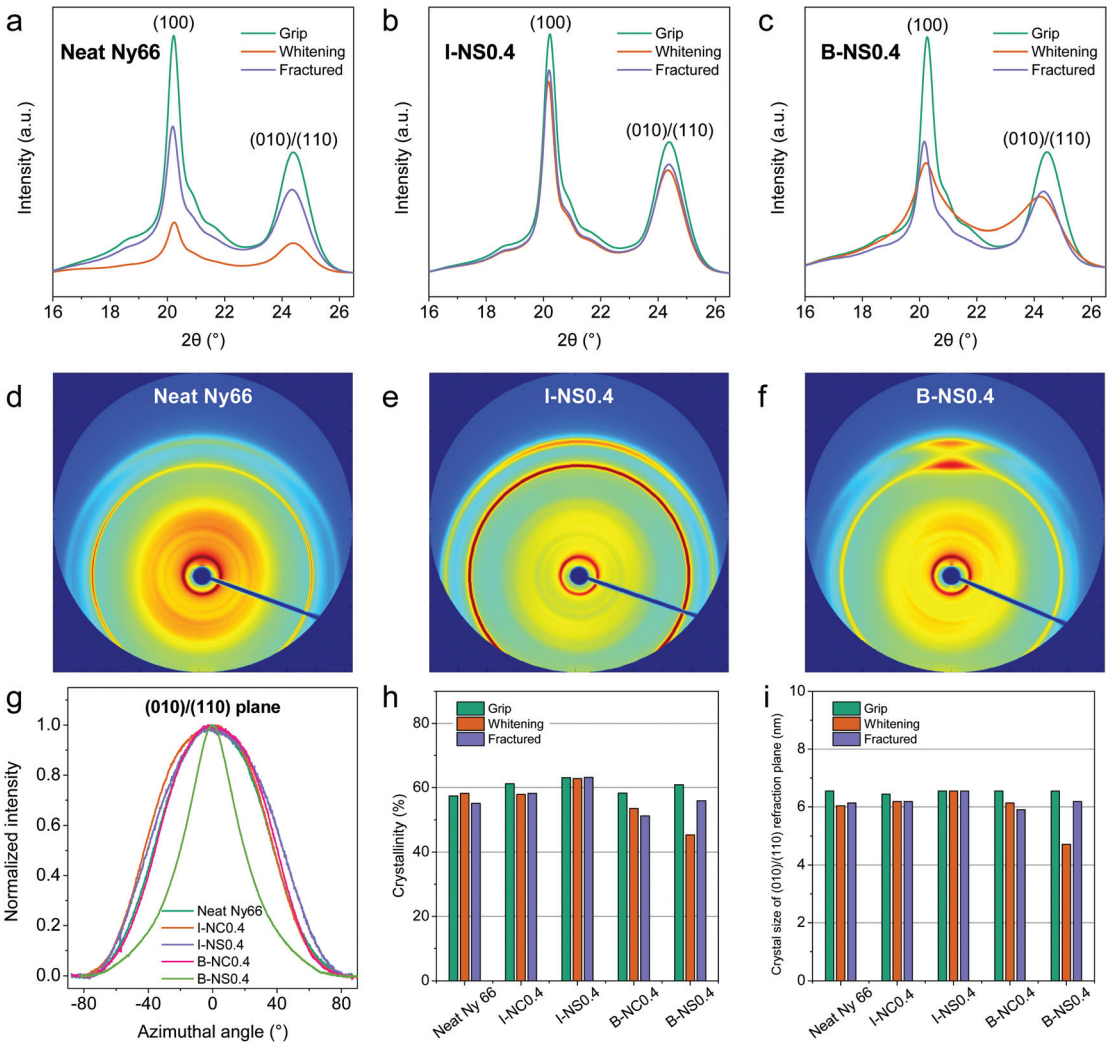

Fig. 4 1D WAXS patterns of (a) neat Ny66, (b) I-NS0.4, and (c) B-NS0.4 films. 2D WAXS profiles at the whitening position of (d) neat Ny66, (e) I-NS0.4, and (f) B-NS0.4 films. (g) Azimuthal scan of the (010)/(110) refraction plane of neat Ny66 film and its nanocomposite films at nanofiller loading of 0.4 wt% at the whitening position. (h) Crystallinity and (i) crystal size of (010)/(110) plane were calculated based on the fitting results of 1D WAXS patterns in Fig. S4 in the ESI.†

Published on 11 November 2019. Downloaded by Korea Research Institute of Chemical Technology (KRICT) on 1/10/2023 6:07:26 AM.

major peaks consists mainly of hydrogen bonding of the aligned polymer chains. The peaks at 20.2 and 24.4°, are assigned to the (100) and the (010)/(110) doublet planes of the α-phase of Ny66 triclinic structure, respectively. The former and latter originate from the intra- and inter-sheet scatterings, respectively.[58] Therefore, the cationic-charged CSW filler, which was incorporated by solution blending helps the polymer matrix relieve the external stress by acting as a plasticizer to facilitate the uniaxial chain extension and dissociation of the intermolecular interaction, resulting in the toughening of the nylon composite. In contrast, the polymeric grafted-CSW filler, which was prepared by the *in situ* method, enhanced the resistance to the uniaxial deformation by preventing the microstructural rearrangement of nylon and thereby produced the stiff composite.

The scattering produces isotropic broad rings in the neat Ny66 and I-NS0.4, even in 2D WAXS patterns at the whitening position (Fig. 4d and e), but rings of much higher intensity were observed in the equatorial region for B-NS0.4 (Fig. 4f), indicating a higher degree of orientation parallel to the stretching direction. The higher orientation of B-NS0.4 was further supported by a narrow distribution in the (010)/(110) Azimuthal scans (Fig. 4g), which agreed well with the extensible property of the B-NS samples. In addition, only B-NS0.4 exhibited a notable change in the crystallinity and crystal size, which indicated that some crystal structures were broken down and the resultant small crystallites were readily aligned along the uniaxial direction (Fig. 4h and i). As expected, the I-NS0.4 sample exhibited little change in these two parameters due to its very high stiffness.

An Azimuthal scan (ψ-scan) of the (010)/(110) refraction plane of neat Ny66 film and its nanocomposite films at nanofiller loading of 0.4 wt% was acquired at the whitening position. The Azimuthal scan consists of a rotation of the crystal structure in the samples around the diffraction vector and the recording of the resulting intensity variations as a function of the rotation angle (ψ). Crystallinity and crystal size of (010)/(110) plane were calculated based on the fitting results of 1D WAXS patterns shown in Fig. S4 in the ESI.†

The interfacial hydrogen bonding of the matrix-filler can be qualitatively assessed by observing the FTIR spectra in the 1700–1450 cm^{-1} region, which show the amide I and II bands (amide I, mainly hydrogen-bonded C═O stretching; amide II, mainly in-plane hydrogen-bonded NH deformation)[59–62] (Fig. 5). The band assignments in the spectral region are summarized in Table S4 in the ESI.† Among the four types of the prepared composite systems, the amide I band (carbonyl) at 1631 cm^{-1} of the I-NS series experienced the greatest red-shift to 1611 cm^{-1} at 0.4 wt% filler loading (Fig. 5b), which verified the strongest interfacial hydrogen bonding in the presence of the grafted Ny66 chains onto the CSW filler.[59,63,64] This result indicated that CSW is a more suitable nanofiller for polyamide composites than CNC due to formation of the stronger interfacial bonding through both chemical and physical interactions by the reactive amine groups on the CSW surface. However, the observed minor peak shift of the B-NS series

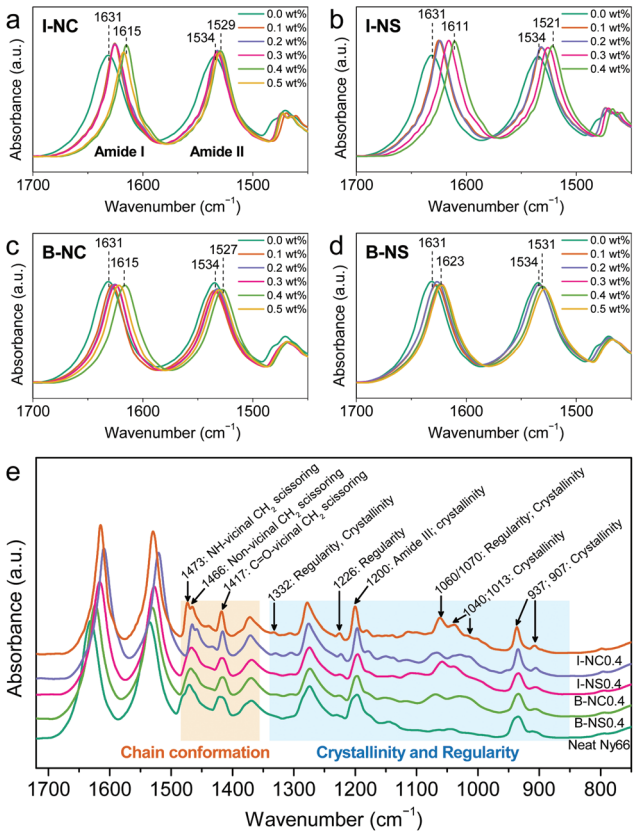

Fig. 5 FTIR spectra in the 1700–1450 cm^{-1} range showing the amide I and II bands for (a) I-NC, (b) I-NS, (c) B-NC, and (d) B-NS nanocomposite films with respect to the filler content. (e) FTIR spectra of the neat Ny66 and its composites at the filler loading of 0.4 wt% over the 1720–750 cm^{-1} range.

could have arisen from different interaction modes of acid-protonated CSW with the Ny66 matrix because the positively charged ammonium groups favor ionic interactions over hydrogen bonding (Fig. 5d).[65,66] In the CNC-containing composites, minor differences in the peak shifting observed between the two series (I-NC and B-NC) suggested that the interfacial interaction mode of CNC was dominantly governed by the physical hydrogen bonding, independent of the preparation methods (Fig. 5a and c). In this regard, the higher mechanically reinforcing efficiency observed in the I-NC seems to originate from a better dispersion of CNC, than that in the post-blended system (B-NC).

It should be noted that in the IR spectra of the composites, the appearance of new minor peaks in the 1500–750 cm^{-1} range indicates the transition to a more stable crystal structure with enhanced structural regularity. These included the bands at 1466 cm^{-1} (amide-non-vicinal CH_2 scissoring), 1332, 1226, 1060, 1040, and 1013 cm^{-1} (*trans*-chain conformation and crystal structure regularity) (Fig. 5e).[59,60,64,67–69] Furthermore, some characteristic bands for the *trans* conformation and crystallinity became sharper in the composite films than in the neat film. These included the bands at 1473 and 1417 cm^{-1},

 This journal is © The Royal Society of Chemistry 2020

Published on 11 November 2019. Downloaded by Korea Research Institute of Chemical Technology (KRICT) on 1/10/2023 6:07:26 AM.

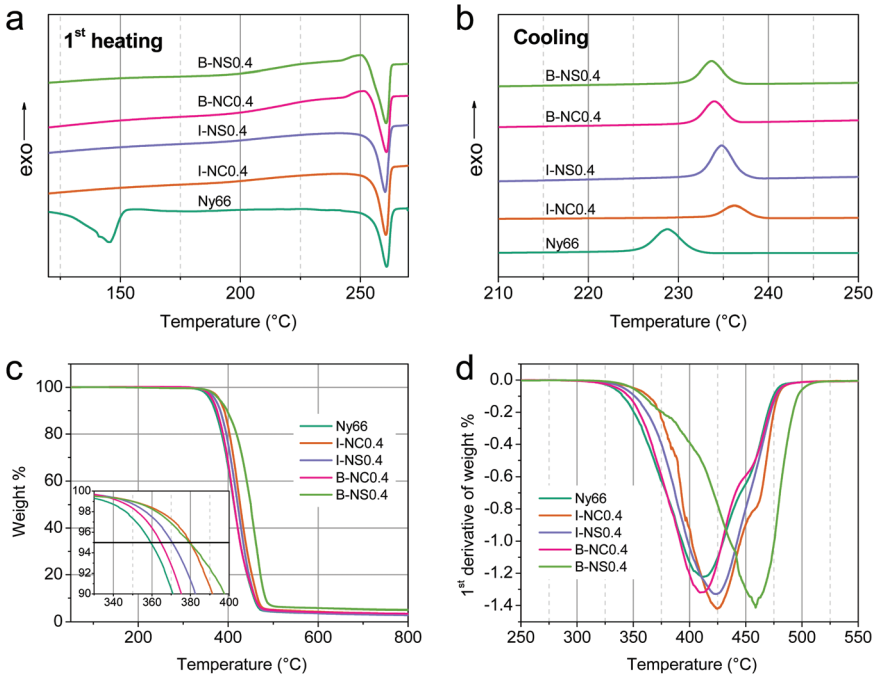

Fig. 6 Thermal properties of neat Ny66 and its composite films at the 0.4 wt% filler loading. DSC of (a) 1st heating and (b) subsequent cooling thermograms of the films. (c) TGA and (d) corresponding differential thermal gravimetric (DTG) curves of the films. The inset figure in (c) presents a magnified view of the onset thermal degradation.

(NH- and CO-vicinal CH_2 scissoring, respectively, and representing the *trans*-chain conformation) and the bands at 1200 and 937 cm^{-1} (representing crystallinity).[59,60,64,70–73] In case of neat Ny66, the structural regularity is dominantly degraded by the Brill structure, which is a less stable, pseudohexagonal crystal, compared with the stable α-triclinic crystal form.[60,69] Overall, these spectral changes in the composite systems suggest that the chain alignment (*trans* conformation) along the filler surface through the interfacial bonding results in the enhanced regularity by minimizing the Brill structure.

Thermal behavior of the Ny66 composites

In the differential scanning calorimetry (DSC) thermogram of the neat Ny66 film, two endothermic peaks appeared at 146 and 261 °C, corresponding to the Brill transition and melting, respectively.[74,75] However, all of the prepared composite films exhibited a melting peak without the Brill endotherm (Fig. 6a). This result is ascribed to the structural conversion from the less-stable pseudohexagonal form to the stable α-triclinic crystal by molecular alignment and interfacial hydrogen bonding along the filler surface, and these results are in agreement with the FTIR results. The complete disappearance of the Brill peak even at the filler loading of 0.1 wt% reveals that the interfacial interaction on the filler surface not only leads to the alignment of the adjacent polymer chains but also affects the structural regularity of the entire matrix (Fig. S6a–d in the ESI†). Higher crystallization temperatures were observed for both CNC and CSW nanocomposite films during cooling, than for neat Ny66, and these values generally increased with an increase in the filler concentration. This trend verified the role of the fillers as effective nucleating agents (Fig. 6b and Fig. S6e–h in the ESI†). The crystallinity (X) was calculated using the equation $X = 100 \times (\Delta H_m / \Delta H_m^\circ)$, where ΔH_m and ΔH_m° (188.4 J g^{-1}) are the melting enthalpies of the composite films and theoretically 100% crystalline Ny66, respectively.[76] Overall, the crystallinity of the composites was slightly higher than that of the neat Ny66, and its value is in the 29–38% range (Table S5 in the ESI†).

Thermal gravimetric analysis (TGA) of the neat Ny66 film revealed that its degradation took place over the 350–500 °C range. The decomposition temperature for 5% weight loss (T_{d5}) was determined to be ~359 °C, and the maximum decomposition temperature (T_{max}) was observed at ~408 °C (Fig. 6c and Table S1 in the ESI†), which are consistent with reported values.[77] The degradation trend of all of the composite films is similar to that of the neat film and showed no separate degradation stage for either CNC[78,79] or CSW,[80] which indicates good dispersion of the nanofiller in the polymer matrix, with minimal aggregation (Fig. S7 in the ESI†). Nonetheless, incorporation of the nanofiller into the polymer matrix even at low concentrations generally improved the thermal stability of the composites, which is attributed to effective filler-matrix interaction though hydrogen bonding or covalent linkage. Interestingly, B-NS samples experienced an unusual elevation in their T_{max}, which reached as high as 460 °C (Fig. 6d), 50 °C higher than that of the pristine film. This increase likely resulted from ionization of CSW by formic acid during the post-blending.[49]

Published on 11 November 2019. Downloaded by Korea Research Institute of Chemical Technology (KRICT) on 1/10/2023 6:07:26 AM.

Conclusions

Inspired by bio-hardening mechanisms in nature, in this study, we fabricated all-organic Ny66 composites using CNC or CSW as nanofillers *via in situ* polymerization or post-solution blending in formic acid. Both these biorenewable nanofillers showed mechanically reinforcing effects on the polymer at considerably low filler loadings (≤0.5 wt%) without the necessity of any surface modification, which is attributed to the matrix-filler interfacial hydrogen bonding. Particularly with CSW, the mechanical properties of the Ny66 composite were freely tunable from being stiff to tough depending on the fabrication technique employed. The Ny66 film was strengthened by *in situ*-incorporated CSW which exhibited σ up to 106 MPa (1.7-fold increase) at 0.4 wt% filler-loading but was toughened by post-blended CSW in formic acid up to 104 MJ m^{-3} (2.1-fold increase) at 0.3 wt%. This versatility of CSW is believed to originate from its amine functional groups, which, not only provide grafting points for Ny66 during *in situ* polymerization, but also undergo formic acid-mediated protonation during solution blending, rendering CSW as a plasticizer. Overall, the outcomes from this research open up possibilities for further development and acceptance of interactive biorenewable nanofiller-based all-organic composites for various industrial applications.

Experimental section

Materials

The monomers, adipoyl chloride (>98%) and hexamethylenediamine (HMDA, >98%), were purchased from TCI (Japan). CNC was purchased from the Process Development Center (University of Maine, US). CSW was prepared from shrimp shell α-chitin (Sigma-Aldrich, US) following an established method.[26] *m*-Cresol (99%), 1,2-dichlorobenzene (99%), formic acid (96%), commercial Ny66 (density 1.14 g mL^{-1}), and sodium hydroxide (NaOH, 97%) were purchased from Sigma-Aldrich. All chemicals were used as received without further purification.

Interfacial polymerization

The polymerization system consisted of two immiscible liquid phases. The organic phase, consisting of adipoyl chloride (6.18 g, 33.8 mmol) in 1,2-dichlorobenzene (200 mL), was allowed to react with the aqueous phase comprising HMDA (4.31 g, 37.1 mmol) in deionized water (400 mL) containing NaOH (3.0 g, 75 mmol), which neutralized the hydrochloric acid byproduct. The organic solution was poured into the aqueous solution under intense stirring, and the mixture was stirred at 35 000 rpm for 5 min using a blender (800 W motor, HR2096/00, Philips, US). The aqueous-to-organic phase volume ratio and the reactant concentrations were optimized for maximizing molecular weight and yield.[47] The polymerization reaction theoretically produces 7.64 g of neat Ny66.

The *in situ* interfacial polymerization of Ny66/CNC and Ny66/CSW composites was conducted with the same reactant ratio as described for the neat Ny66. The nanofillers *i.e.*, CNC or CSW were dispersed in the aqueous phase by homogenization at 5000 rpm for 10 min using a homogenizer (T 25 digital ULTRA-TURRAX®, IKA, Germany), followed by bath-sonication using an Ultrasonic Cleaner (SD-D400H, LKLABKOREA Inc., South Korea) at 50% amplitude for 30 min at 25 °C. The percentages of the nanofillers were 0.1–0.5 wt% with respect to the theoretical yield of Ny66 composites.

All products were subjected to a two-stage purification process. The products were first washed repeatedly with methanol to remove by-products, unreacted monomers, and the solvents, and were then filtered through a Büchner funnel and vacuum-dried at 80 °C for 12 h. In the second stage, the dried product was cryo-pulverized in liquid nitrogen for 10 min and then bath-sonicated in methanol at 50% amplitude for 30 min. The cryo-grinding and sonication increased the contaminant extraction efficiency with methanol. The processes were repeated three times.

Preparation of nanocomposite films

Films were prepared using a solution casting method. Ny66 or its *in situ*-generated nanocomposites were dissolved in formic acid and were stirred for 2 days at 25 °C to produce 6.5 wt% solutions. Solution-blended Ny66 nanocomposite solutions were prepared separately, according to the following procedure. The as-synthesized neat Ny66 was dissolved in formic acid (6.5 wt%) and upon achieving complete dissolution of the polymer, the natural organic nanofillers, which were CNC or CSW, were added into the solutions at different weight percentages (0.1–0.5 wt%, compared to the Ny66 composite). The nanofillers were dispersed in the nylon solutions by bath sonication at 50% amplitude for 2 h and were then allowed to rest for 24 h. Further bath sonication was carried out again at 50% amplitude for 2 h. The film was obtained by pouring the homogenous solution into a glass Petri dish (15 mL per Petri dish with a diameter of 90 mm) followed by evaporation for 5 days. The solvent evaporation rate was reduced by placing an inverted glass funnel over the Petri dish, which reduced the exposure of the solution to the atmosphere. The formed films were then vacuum dried at 80 °C overnight to ensure complete removal of the residual solvent.

In order to study the effect of the solvent evaporation rate on the properties of resulting composite films, in a separate film processing experiment, the funnel was removed after 24 h, so that formic acid could evaporate within the next 24 h. The film thus formed in 2 days was dried under vacuum at 80 °C overnight to remove the residual solvent, and the film's mechanical properties and morphology were compared with those that were formed under slow solvent evaporation.

Characterization

M_V of Ny66 and its nanocomposites was determined by viscometry using a type II Ubbelohde capillary viscometer with a kinematic viscosity constant of 0.09944 mm^2 s^{-2} (ISO 307).

 This journal is © The Royal Society of Chemistry 2020

Published on 11 November 2019. Downloaded by Korea Research Institute of Chemical Technology (KRICT) on 1/10/2023 6:07:26 AM.

The flow time of polymer solutions in *m*-cresol was measured at concentrations of 0.2–1 g dL^{-1} at 25 °C after they were syringe-filtered through a hydrophobic polytetrafluoroethylene membrane (pore size diameter: 0.45 μm). The relative viscosity was calculated from the ratio of the flow time of the polymer solution to that of the pure solvent, assuming that all solutions have the same density at low concentration. The specific viscosity and reduced viscosity were calculated from the relative viscosity[81] and were then plotted as a function of concentration. The intrinsic viscosity was then determined from the obtained plot. The Mark–Houwink equation $[\eta] = KM^{\alpha}$ (where $[\eta]$ and M are intrinsic viscosity and viscosity average molecular weight, respectively; $K = 2.4 \times 10^{-3}$ and $\alpha = 0.61$ for Ny66 in *m*-cresol at 25 °C)[81] were used to determine the M_V of Ny66 composites.

The mechanical properties of the films were tested on a universal testing machine (Model 5943, Instron, UK) at 25 °C. The films used for the tensile test were cut into a dumbbell shape following the ASTM D638 Type 1 standard. All samples were conditioned in a controlled-atmosphere chamber at 25 °C and a 50% relative humidity for 48 h before testing.

The degradation temperature of the films was evaluated using TGA (Pyris 1, PerkinElmer, US). The samples were preconditioned for complete moisture removal. Measurement was then conducted by heating the films from 30 °C to 800 °C at a 10 °C min^{-1} rate under a dry nitrogen atmosphere, with a flow rate of 20 mL min^{-1}.

DSC measurements were carried out using a DSC Q2000 calorimeter (TA Instruments Inc., US) under a dry nitrogen atmosphere, with a flow rate of 20 mL min^{-1}. The nanocomposite films (~1.4–2.0 mg) were placed in the aluminum sample pans after complete moisture removal. The samples were heated from 30 °C to 280 °C, and subsequently cooled down to 0 °C. All thermal scans were performed at a 10 °C min^{-1} rate, and the samples were kept isothermal for 5 min at the beginning of each thermal cycle.

Attenuated total reflectance Fourier-transform infrared spectroscopy (ATR-FTIR) spectra were recorded using a Nicolet™ iS50 FTIR spectrometer (Thermo Scientific, US) with a smart iTR diamond ATR accessory (face angle: 45°). For each spectrum, a total of 256 scans at a scan step of 2 cm^{-1} over a range of 4000–400 cm^{-1} were collected.

A field-emission SEM (MIRA3, Tescan, Czech Republic) with a secondary electron detector was employed to observe the morphology of Ny66 nanocomposite films after tensile testing at three positions, which were (1) the unstressed film surface of the grip section, (2) the whitening area of necking-position, and (3) the cross-sectional area of the fractured position. The samples were coated with a thin layer of Pt (~7 nm) using a Q150 T Plus turbomolecular pumped coater (Quorum Technologies Ltd, UK), which was operated at 15 mA for 90 s before SEM observation.

SAXS/WAXS measurements were carried out using synchrotron radiation at the wavelength of 1.28 Å generated at the 3C SAXS I Beamline, Pohang Accelerator Laboratory. The sample-to-detector distance was set as 2090 mm.

Conflicts of interest

There are no conflicts to declare.

Acknowledgements

This work was supported by the Technology Innovation Program (10070150) funded by the Ministry of Trade, Industry & Energy (MI, Korea) and Korea Research Institute of Chemical Technology (KRICT) core project. S. Y. H. acknowledges support from Basic Science Research Program through the National Research Foundation of Korea (NRF) funded by the Ministry of Science, ICT & Future Planning (2018R1C1B6002344). L. T. H. acknowledges Mr Nguyen Hoang Linh (Pohang University of Science and Technology) for his basic guidance in nylon composite and film processing. We acknowledge the Pohang Accelerator Laboratory for X-ray diffraction measurements with synchrotron radiation (Beamline 3C).

References

1 R. C. Thompson, S. H. Swan, C. J. Moore and F. S. vom Saal, *Philos. Trans. R. Soc., B*, 2009, **364**, 1973–1976.
2 Editorial, *Nat. Commun.*, 2018, **9**, 2157.
3 S.-A. Park, H. Jeon, H. Kim, S.-H. Shin, S. Choy, D. S. Hwang, J. M. Koo, J. Jegal, S. Y. Hwang, J. Park and D. X. Oh, *Nat. Commun.*, 2019, **10**, 2601.
4 P. Judeinstein and C. Sanchez, *J. Mater. Chem.*, 1996, **6**, 511–525.
5 C. Sanchez, C. Boissiere, S. Cassaignon, C. Chaneac, O. Durupthy, M. Faustini, D. Grosso, C. Laberty-Robert, L. Nicole, D. Portehault, F. Ribot, L. Rozes and C. Sassoye, *Chem. Mater.*, 2014, **26**, 221–238.
6 M. Faustini, L. Nicole, E. Ruiz-Hitzky and C. Sanchez, *Adv. Funct. Mater.*, 2018, **28**, 1704158.
7 S. Y. Hwang, W. D. Lee, J. S. Lim, K. H. Park and S. S. Im, *J. Polym. Sci., Part B: Polym. Phys.*, 2008, **46**, 1022–1035.
8 G. Mittal, V. Dhand, K. Y. Rhee, S.-J. Park and W. R. Lee, *J. Ind. Eng. Chem.*, 2015, **21**, 11–25.
9 C. Harito, D. V. Bavykin, B. Yuliarto, H. K. Dipojono and F. C. Walsh, *Nanoscale*, 2019, **11**, 4653–4682.
10 J. Hopewell, R. Dvorak and E. Kosior, *Philos. Trans. R. Soc., B*, 2009, **364**, 2115–2126.
11 J. N. Hahladakis, C. A. Velis, R. Weber, E. Iacovidou and P. Purnell, *J. Hazard. Mater.*, 2018, **344**, 179–199.
12 C. R. Estrellan and F. Iino, *Chemosphere*, 2010, **80**, 193–207.
13 C. Buzea, I. I. Pacheco and K. Robbie, *Biointerphases*, 2007, **2**, MR17–MR71.
14 A. Nel, T. Xia, L. Mädler and N. Li, *Science*, 2006, **311**, 622–627.
15 E. Manias, *Nat. Mater.*, 2007, **6**, 9.
16 S. K. Kumar, N. Jouault, B. Benicewicz and T. Neely, *Macromolecules*, 2013, **46**, 3199–3214.

Published on 11 November 2019. Downloaded by Korea Research Institute of Chemical Technology (KRICT) on 1/10/2023 6:07:26 AM.

17 B. Di Credico, E. Cobani, E. Callone, L. Conzatti, D. Cristofori, M. D'Arienzo, S. Dirè, L. Giannini, T. Hanel, R. Scotti, P. Stagnaro, L. Tadiello and F. Morazzoni, *Appl. Clay Sci.*, 2018, **152**, 51–64.
18 P. Akcora, H. Liu, S. K. Kumar, J. Moll, Y. Li, B. C. Benicewicz, L. S. Schadler, D. Acehan, A. Z. Panagiotopoulos, V. Pryamitsyn, V. Ganesan, J. Ilavsky, P. Thiyagarajan, R. H. Colby and J. F. Douglas, *Nat. Mater.*, 2009, **8**, 354–359.
19 A. Šturcová, G. R. Davies and S. J. Eichhorn, *Biomacromolecules*, 2005, **6**, 1055–1061.
20 J. F. V. Vincent and U. G. K. Wegst, *Arthropod Struct. Dev.*, 2004, **33**, 187–199.
21 E. Hirose, S. Kimura, T. Itoh and J. Nishikawa, *Biol. Bull.*, 1999, **196**, 113–120.
22 D. Trache, M. H. Hussin, M. K. M. Haafiz and V. K. Thakur, *Nanoscale*, 2017, **9**, 1763–1786.
23 Y. Van Daele, J.-F. Revol, F. Gaill and G. Goffinet, *Biol. Cell*, 1992, **76**, 87–96.
24 A. Miserez, T. Schneberk, C. Sun, F. W. Zok and J. H. Waite, *Science*, 2008, **319**, 1816–1819.
25 T. Kim, H. Jeon, J. Jegal, J. H. Kim, H. Yang, J. Park, D. X. Oh and S. Y. Hwang, *RSC Adv.*, 2018, **8**, 15389–15398.
26 T. H. Tran, H.-L. Nguyen, D. S. Hwang, J. Y. Lee, H. G. Cha, J. M. Koo, S. Y. Hwang, J. Park and D. X. Oh, *Carbohydr. Polym.*, 2019, **205**, 392–400.
27 T. H. Tran, H.-L. Nguyen, L. T. Hao, H. Kong, J. M. Park, S.-H. Jung, H. G. Cha, J. Y. Lee, H. Kim, S. Y. Hwang, J. Park and D. X. Oh, *Int. J. Biol. Macromol.*, 2019, **125**, 660–667.
28 J. J. Richardson, B. L. Tardy, J. Guo, K. Liang, O. J. Rojas and H. Ejima, *ACS Sustainable Chem. Eng.*, 2019, **7**, 6287–6294.
29 Y. Habibi, L. A. Lucia and O. J. Rojas, *Chem. Rev.*, 2010, **110**, 3479–3500.
30 B. Vollick, P.-Y. Kuo, H. Thérien-Aubin, N. Yan and E. Kumacheva, *Chem. Mater.*, 2017, **29**, 789–795.
31 J.-B. Zeng, Y.-S. He, S.-L. Li and Y.-Z. Wang, *Biomacromolecules*, 2012, **13**, 1–11.
32 X. Zhang and M. Rolandi, *J. Mater. Chem. B*, 2017, **5**, 2547–2559.
33 A. C. Corrêa, E. de Morais Teixeira, V. B. Carmona, K. B. R. Teodoro, C. Ribeiro, L. H. C. Mattoso and J. M. Marconcini, *Cellulose*, 2014, **21**, 311–322.
34 H. Oliver-Ortega, L. A. Granda, F. X. Espinach, J. A. Mendez, F. Julian and P. Mutjé, *Compos. Sci. Technol.*, 2016, **132**, 123–130.
35 H. Yousefian and D. Rodrigue, *Polym. Compos.*, 2016, **37**, 1473–1479.
36 Cellulose nanocrystals (CNC) – Product Specification, https://umaine.edu/pdc/wp-content/uploads/sites/398/2016/03/Specs-CNC.pdf, (accessed Dec 19, 2018).
37 Y. Eom, S. M. Son, Y. E. Kim, J.-E. Lee, S.-H. Hwang and H. G. Chae, *Carbon*, 2019, **150**, 142–152.
38 E. D. Smith, K. D. Hendren, J. V. Haag, E. J. Foster and S. M. Martin, *Nanomaterials*, 2019, **9**, 125.
39 T. E. Motaung, M. J. Mochane, Z. L. Linganiso and A. P. Mashigo, *Polym. Sci.*, 2017, **3**, 1.
40 S. Kashani Rahimi and J. U. Otaigbe, *Polym. Eng. Sci.*, 2016, **56**, 1045–1060.
41 S.-A. Park, Y. Eom, H. Jeon, J. M. Koo, E. S. Lee, J. Jegal, S. Y. Hwang, D. X. Oh and J. Park, *Green Chem.*, 2019, **21**, 5212–5221.
42 J. M. Koo, J. Kang, S.-H. Shin, J. Jegal, H. G. Cha, S. Choy, M. Hakkarainen, J. Park, D. X. Oh and S. Y. Hwang, *Compos. Sci. Technol.*, 2020, **185**, 107885.
43 R. Haggenmueller, F. Du, J. E. Fischer and K. I. Winey, *Polymer*, 2006, **47**, 2381–2388.
44 M. Kang, S. J. Myung and H.-J. Jin, *Polymer*, 2006, **47**, 3961–3966.
45 M. Moniruzzaman, J. Chattopadhyay, W. E. Billups and K. I. Winey, *Nano Lett.*, 2007, **7**, 1178–1185.
46 R. Sengupta, A. Ganguly, S. Sabharwal, T. K. Chaki and A. K. Bhowmick, *J. Mater. Sci.*, 2007, **42**, 923–934.
47 Z. S. Kalkan and L. A. Goettler, *Polym. Eng. Sci.*, 2009, **49**, 1491–1501.
48 C. Honorato-Rios, C. Lehr, C. Schütz, R. Sanctuary, M. A. Osipov, J. Baller and J. P. F. Lagerwall, *NPG Asia Mater.*, 2018, **10**, 455–465.
49 M. Nagalakshmaiah, N. El Kissi and A. Dufresne, *ACS Appl. Mater. Interfaces*, 2016, **8**, 8755–8764.
50 E. L. Papadopoulou, F. Pignatelli, S. Marras, L. Marini, A. Davis, A. Athanassiou and I. S. Bayer, *RSC Adv.*, 2016, **6**, 6823–6831.
51 M. L. Berins, in *SPI Plastics Engineering Handbook of the Society of the Plastics Industry, Inc*, ed. M. L. Berins, Springer US, Boston, MA, 1991, ch. 3, pp. 47–78.
52 J. A. Brydson, in *Plastics Materials (Seventh Edition)*, ed. J. A. Brydson, Butterworth-Heinemann, Oxford, 1999, ch. 18, pp. 478–530.
53 A. Chakrabarty and Y. Teramoto, *Polymers*, 2018, **10**, 517.
54 K. Oksman, Y. Aitomäki, A. P. Mathew, G. Siqueira, Q. Zhou, S. Butylina, S. Tanpichai, X. Zhou and S. Hooshmand, *Composites, Part A*, 2016, **83**, 2–18.
55 T. Hanemann and D. V. Szabó, *Materials*, 2010, **3**, 3468–3517.
56 J. M. Koo, H. Kim, M. Lee, S.-A. Park, H. Jeon, S.-H. Shin, S.-M. Kim, H. G. Cha, J. Jegal, B.-S. Kim, B. G. Choi, S. Y. Hwang, D. X. Oh and J. Park, *Macromolecules*, 2019, **52**, 923–934.
57 W. O. Statton, *J. Polym. Sci.*, 1962, **58**, 205–220.
58 N. Klein, G. Marom and E. Wachtel, *Polymer*, 1996, **37**, 5493–5498.
59 C. G. Cannon, *Spectrochim. Acta*, 1960, **16**, 302–319.
60 S. J. Cooper, M. Coogan, N. Everall and I. Priestnall, *Polymer*, 2001, **42**, 10119–10132.
61 Y. Ma, T. Zhou, G. Su, Y. Li and A. Zhang, *RSC Adv.*, 2016, **6**, 87405–87415.
62 I. Sandeman and H. W. Thompson, *Proc. R. Soc. London, Ser. A*, 1955, **232**, 105–113.

 This journal is © The Royal Society of Chemistry 2020

Published on 11 November 2019. Downloaded by Korea Research Institute of Chemical Technology (KRICT) on 1/10/2023 6:07:26 AM.

63 N. B. Colthup, L. H. Daly and S. E. Wiberley, in *Introduction to Infrared and Raman Spectroscopy (Third Edition)*, ed. N. B. Colthup, L. H. Daly and S. E. Wiberley, Academic Press, San Diego, 1990, ch. 9, pp. 289–325.
64 D. Galimberti, C. Quarti, A. Milani, L. Brambilla, B. Civalleri and C. Castiglioni, *Vib. Spectrosc.*, 2013, **66**, 83–92.
65 T. Steiner, *Angew. Chem., Int. Ed.*, 2002, **41**, 48–76.
66 G. A. Jeffrey and W. Saenger, in *Hydrogen Bonding in Biological Structures*, Springer Berlin Heidelberg, Berlin, Heidelberg, 1991, ch. 14, pp. 220–231.
67 C. G. Cannon and P. H. Harris, *J. Macromol. Sci., Part B: Phys.*, 1969, **3**, 357–364.
68 J. L. Koenig and M. C. Agboatwalla, *J. Macromol. Sci., Part B: Phys.*, 1968, **2**, 391–420.
69 N. Vasanthan, N. S. Murthy and R. G. Bray, *Macromolecules*, 1998, **31**, 8433–8435.
70 I. Matsubara and J. H. Magill, *Polymer*, 1966, **7**, 199–215.
71 N. Vasanthan and D. R. Salem, *J. Polym. Sci., Part B: Polym. Phys.*, 2000, **38**, 516–524.
72 N. Vasanthan and D. R. Salem, *Mater. Res. Innovations*, 2001, **4**, 155–160.
73 D. Garcia and H. W. Starkweather Jr., *J. Polym. Sci., Polym. Phys. Ed.*, 1985, **23**, 537–555.
74 A. Y. Feldman, E. Wachtel, G. B. M. Vaughan, A. Weinberg and G. Marom, *Macromolecules*, 2006, **39**, 4455–4459.
75 C. Ramesh, A. Keller and S. J. E. A. Eltink, *Polymer*, 1994, **35**, 2483–2487.
76 E. Chi, M. An, G. Yao, F. Tian and Z. Wang, *Crystals*, 2017, **7**, 384.
77 A. Attanasio, I. S. Bayer, R. Ruffilli, F. Ayadi and A. Athanassiou, *ACS Appl. Mater. Interfaces*, 2013, **5**, 5717–5726.
78 J. Gong, J. Li, J. Xu, Z. Xiang and L. Mo, *RSC Adv.*, 2017, **7**, 33486–33493.
79 N. Wang, E. Ding and R. Cheng, *Polymer*, 2007, **48**, 3486–3493.
80 A. G. B. Pereira, E. C. Muniz and Y.-L. Hsieh, *Carbohydr. Polym.*, 2014, **107**, 158–166.
81 J. J. Burke and T. A. Orofino, *J. Polym. Sci., Part A-2*, 1969, **7**, 1–25.